Atmos. Chem. Phys. Discuss., 3, 733–768, 2003
www.atmos-chem-phys.org/acpd/3/733/

Atmospheric Chemistry and Physics Discussions

Effects of various meteorological conditions and spatial emission resolutions on the ozone concentration & ROG/NO_x limitation in the Milan area (I)

N. Bärtsch-Ritter, J. Keller, J. Dommen, and A. S. H. Prévôt

Paul Scherrer Institute, Laboratory of Atmospheric Chemistry, CH-5232 Villigen PSI, Switzerland

Received: 23 December 2003 – Accepted: 30 January 2003 – Published: 12 February 2003

Correspondence to: A. S. H. Prévôt (andre.prevot@psi.ch)

Abstract

The three-dimensional photochemical model UAM-V is used to investigate the effects of various meteorological conditions and of the coarseness of emission inventories on the ozone concentration and ROG/NO_x limitation of the ozone production in the Po Basin in the northern part of Italy. As a base case, the high ozone episode with up to 200 ppb on 13 May 1998 was modelled and previously thoroughly evaluated with measurements gained during a large field experiment. The performed variations in meteorology are applied to mixing height, air temperature, specific humidity and wind speed. Three coarser emission inventories are obtained by resampling from $3 \times 3\,km^2$ up to $54 \times 54\,km^2$ emission grids. The model results show that changes in meteorological input files have the largest effect on peak ozone. In the modelled ozone plume a slope of 10.1 ppb ozone/° C and in Milan of 2.8 ppb ozone/° C were found. The net ozone formation in northern Italy is more strongly temperature than humidity dependent, while the humidity is very important for the ROG/NO_x limitation of the ozone production. For each of the meteorological variations (e.g. doubling the mixing height), the modelled ozone plume remains ROG limited for this case. A strong change towards NO_x sensitivity in the ROG limited areas is only found if much coarser emission inventories were applied. Increasing ROG limited areas with increasing wind speed are found, because the ROG limited ozone chemistry induced by point sources is spread over a larger area. Simulations without point sources tend to increase the NO_x limited areas.

1. Introduction

In the troposphere, ozone is formed through various chemical reactions involving NO_x ($NO + NO_2 = NO_x$), reactive organic gases (ROG) and sunlight with non-linear dependencies (Lin et al., 1988; Sillman, 1999). In addition, ozone formation is heavily sensitive to meteorological fluctuations as well as to changes in precursor emissions

ACPD

3, 733–768, 2003

(NO_x and ROG) (Brönnimann et al., 2002; Brönnimann and Neu, 1997; Wolff et al., 2001).

In Europe and the U.S., several studies have been performed analysing the impact of meteorological factors on measured ozone (Bloomfield et al., 1996; Davis et al., 1998) or simulated ozone concentrations (Sillman and Samson, 1995; Khalid and Samson, 1996; Brönnimann and Neu, 1997). Different authors used photochemical models and/or analysed the effects with the help of statistical analyses (Andreani-Aksoyoglu and Keller, 1996; Sistla et al., 1996; Porter et al., 2001). Other model studies showed the effect of the emission on the ozone formation using different grid sizes (Jang et al., 1995; Li et al., 1998). But hardly any information can be found about the dependence of the ROG and NO_x sensitivity of the ozone production on meteorological variability.

The major errors in photochemical modelling evolve from unsatisfactory input of the meteorology and emissions (Russel and Dennis, 2000). Hence, great attention to most "realistic" inputs should be laid. Adjustments in input files should be considered after a careful evaluation of the model results with regard to a wide range of measurements. Often, only modelled ozone concentrations are compared to measurements and may simply agree by accident. It is well known, that different ROG/NO_x ratios may lead to the same ozone production. As a consequence, the interpretation of the limitation may lead to no adequate ozone control strategies. Incorrectness of meteorological input parameters may lead as well to changed ozone predictions and limitation, as will be shown.

Bärtschi-Ritter et al. (2003) described a pollution episode and its limitation in the Milan area (I) on 13 May 1998 using a modified emission inventory. The modification yielded particularly in the ozone plume a good agreement with observation. Measurements showed that peroxide concentration in the ozone plume decreased where peak ozone occurred. However, first model simulations indicated the contrary. Sillman (1995) emphasised that the hydrogen peroxide production is very sensitive to NO_x or ROG limited ozone production conditions. A thorough evaluation of ratios found in the original emission inventory compared to measurements gained during the PIPAPO

field experiment (Pianura Padana Produzione di Ozono) (Neftel et al., 2002) led to the modification (Dommen et al., 2003; Bärtschi-Ritter et al., 2003). More confidence is achieved using the modified emission inventory for the model simulations and question of limitation. The case of 13 May 1998 with the modified emission inventory is a good base case for the study of model sensitivity, primarily because of the good agreement with the measurements. The simulation period is 12–13 May 1998 with one additional start-up day to limit the influence of the initial concentrations. The results are discussed for 13 May 1998, 15:00 CET.

This paper deals with the sensitivity on the ozone production affected under meteorological changes and coarser emissions applied on this well described and evaluated modelled pollution episode mentioned above. The focus is laid on the meteorology on different mixing heights, air temperatures, specific humidities and wind speeds and on various coarse emission inventories by resampling the modified emissions. Several point sources are included in the model simulations affecting the modelling domain particularly. This paper may especially contribute to a better understanding of the tendency of the resulting limitations affected by changes in meteorology and spatial resolution of emission inventories.

2. Area of investigation

The area of investigation – the northern part of Italy – is given as a black-white extract of a true-colour MODIS image (http://modis.gsfc.nasa.gov), which was acquired from data collected on 11 October 2001 (Fig. 1). In the southern part of the scene the flat "Po Basin" with the city of Milan (thick circle) and the surrounding suburbs are visible. Roughly 9 million people are living in this large, densely populated and highly industrialized urban area. The Po Basin is rather flat, with an average altitude of 100 m a.s.l. To the north of Milan, the altitude increases, reaching the Prealps (in the vicinity of the lakes, dark black areas) and the Alps in the most northern part of the satellite scene. The latter surpass over 3000 m a.s.l., around 150 km from Milan and are covered by

snow and ice (white areas). Circles indicate Milan centre and the representative urban measurement station Bresso. Seven large point sources, mainly power stations and refineries, are marked by triangles, which are treated explicitly in the model simulations.

3. Model description

System Application International (SAI) developed a three-dimensional photochemical model referred as Urban Airshed Model with variable grid (UAM-V). The UAM-V incorporates two-way, horizontal and vertical multiple grid nesting, a plume-in-grid treatment of elevated point source emissions, dry deposition and three-dimensional meteorological input data (SAI, 1999). The model allows the description of regional-scale processes, simulating the effects of emissions, diffusion, advection, chemical transformation and surface removal processes. The chemistry is described by the Carbon Bond Mechanism IV (CBM-IV), which includes 94 chemical reactions (Gery et al., 1989). The reaction rate constants in the model were updated based on (Atkinson et al., 1997). In the original model version 1.15, an incorrect formulation of the transport schemes was detected. The model was then improved (Keller et al., 2002), which now is used in this presented model study.

The meteorology of the base case was calculated with the meteorological pre-processor SAIMM (SAI Mesoscale Model: SAI, 1995). This model comes along with the UAM-V package and includes a set of utility programs for input preparation and data conversion between the meteorological and chemical model. We run SAIMM with 19 layers and an extended domain (243 km × 264 km) to limit the influences at the boundaries of the modelling domain. The meteorological pre-processor provides five meteorological input files that UAM-V requires (wind speed, temperature, water vapour, vertical turbulent exchange coefficient (k_v) and height/pressure).

The meteorological mesoscale model package is based on the hydrostatic model MM2 (Pielke, 1974). SAIMM is no “real” prognostic model but rather a hybrid. Observed temperature, moisture and wind data can be incorporated into the meteorologi-

cal model using four-dimensional data assimilation. The model employs the Newtonian relaxation or "nudging" technique in which one or more of the time-dependent variables are relaxed or "nudged" toward observed values that are spatially weighted during the course of the simulation (SAI, 1995). Thus, this technique should provide more accurate meteorological fields for use in air-quality modelling.

The meteorological simulation for the base case was done from 9–13 May. For the initialisation and the four-dimensional data assimilation, hourly surface data were taken from the monitoring network ANETZ operated by MeteoSwiss and from several ground stations operated during the PIPAPO field experiment. Information about upper air levels were available every 6 h from balloon soundings at Linate airport and every hour from a wind profiler in Seregno, 15 km north of Milan. The model was "nudged" towards these observed values. Realistic surface wind fields with 2–3 m/s in the Po Basin were reproduced by SAIMM, whereas the mixing layer height was overestimated. From airplane measurements it is known that the mixing layer on 13 May was about 1100–1200 m a.s.l. Thus, the mixing layer height was restricted to the top of the fourth model layer (1000 m a.g.l.) by adjusting the vertical profile of the vertical turbulent exchange coefficients (Bärtsch-Ritter et al., 2003).

3.1. Model domain

The photochemical model simulations were performed in the so-called LOOP domain with a 3 km × 3 km resolution. The west-east and north-south extension of the domain is 141 km and 162 km, respectively (see dashed rectangle in Fig. 1). Eight vertical terrain following atmospheric layers were used extending from the surface up to 3000 m a.g.l. The layers mid-points are found at 25, 100, 325, 750, 1250, 1750, 2250 and 2750 m a.g.l.

3.2. Meteorological situation

The meteorological situation during the episode in May 1998 was favourable for high photooxidant production: clear sky, stagnant weather condition, high irradiance and temperatures which were governed by a stationary high-pressure ridge at 500 hPa extending from north Africa to southern Scandinavia. Daily temperatures in Milan exceeded 30° C on 12 and 13 May. In the late afternoon of the second day, high convective clouds developed in the mountains leading to thunderstorms and terminating the nice weather period. In the base case (*bc*), the maximum mixing height during daytime was 1000 m a.g.l. Near the ground, the air temperature (T) at Milan centre at 15:00 CET was around 29° C with a specific humidity (q) of 8.2 g/kg, which corresponds to about 32% relative humidity. The pollution episode on 13 May 1998 occurred under relatively dry conditions. The wind speed (v) in the Po Basin during daytime was around 2–3 m/s.

4. Design of various meteorological conditions

Sensitivity analyses to the three-dimensional meteorological fields in the well described and observation close base case (*bc*) are performed. Five major cases were designed: Change of the mixing height (A), air temperature (B) and specific humidity (C) variations, individual combination of case B and C (D) and enhancement of the wind speed (E). Detailed information about the five cases are given in Table 1.

Within one case, different variations were simulated. The variations of the cases A–D could be directly prepared. The three-dimensional meteorological fields were scaled as a whole, maintaining the vertical and horizontal differences. To increase the temperature by 2° C as an example, the original three-dimensional temperature field of the *bc* was changed by adding 2° C in each grid cell.

The daily maximum of the original mixing height, 1000 m a.g.l., was increased twice by 500 m. The maximum of the well-mixed boundary layer in A1 has now an extension

ACPD
3, 733–768, 2003

of around 1500 m and in A2 of 2000 m.

In variations B1–B7, the original temperature field was varied with a ΔT of −4, −2, 2, 4, 6, 8, 10° C and in variations D1–D5 with ΔT of 2, 4, 6, 8, 10° C. The undertaken variations of the original specific humidity field in variations C1–C8 are −60, −50, −40, −30, −20, −10, 10, 20% and in variations D1–D5 20, 45, 65, 90 and 110%. In variations D1–D5, the temperature enhancement was combined with a humidity increase. The humidity was increased maximally without exceeding 95% relative humidity during night. At 15:00 CET, the relative humidity for these variations is still low at Milan with around 34 to 38%. In Table 1, only results of the extreme variations of the cases B, C, and D are shown.

The preparation of the meteorological fields for variations E1–E2 was performed with SAIMM, assuring mass conservation. This means, that mass conservation in the meteorological model satisfy some discrete form of the continuity equation, which otherwise could lead to an inconsistency with the air quality model. In SAIMM, all available wind input information were enhanced for every simulated day until 12:00 CET by a factor of 2 or 5 and used during the "nudging". The resulting meteorological input files from SAIMM were used for the model simulations.

5. Design of various spatially coarser emission inventories

The emission inventory (EI) compiled in the CBM-IV mechanism was modified according to measurements during the PIPAPO campaign (Dommen et al., 2003) and is used here for the base case. It contains 5 inorganic (NO, NO_2, N_2O_5, CO, SO_2) and 12 ROG species (HCHO, ALD2, PAR, OLE, ETH, TOL, CRES, XYL, ISOP, MEOH, ETOH and METH) (Gery et al., 1989). All presented simulations are run on the basis of a 3 km × 3 km grid size resolution of the emission inventory.

The resampling of EI to a spatially coarser inventory was performed in a simple way. The chosen resampling sizes of the new emission inventories are 9 × 9 km^2, 27 × 27 km^2 and 54 × 54 km^2, common multiples of the original grid size (Table 1, cases F

ACPD
3, 733–768, 2003

and G). EI was resampled over the new chosen sizes and the according means were redistributed back into new emission inventory files with the original grid size. Retaining the original grid size resolution required no recalculation of the meteorological input files and leads to no loss of details, as is reported by (Kumar et al., 1994). In this way, the effect of the coarser emissions on the modelled concentrations in the domain can be studied isolated. The meteorology at a coarser grid would lead to an additional modification of the modelled concentrations.

The applied upscaling technique obviously reduces the emission variability of the highest emission grid cells in the city with the surrounding grid cells. The variations of the highest NO emission grid cell for Milan at different hours are given in Table 2. During one of the busy morning rush hours (08:00–09:00 CET) the NO emission drops to 33%, 68% and to 87% of the original maximum emission when enlarging the spatial resolution of the emissions to $9 \times 9\,km^2$, $27 \times 27\,km^2$ and to $54 \times 54\,km^2$, respectively.

In the variations of case F (as in the cases A–D), the point sources were treated explicitly. The design of the variations G1–G3, where no point sources are implemented during the model simulations, is used to investigate the influence of explicitly treated point sources in different coarser inventory model runs.

6. Results and discussion

Model simulations for all designed variations of the major cases A–G (Table 1) were performed. In addition to each simulation, ROG or NO_x reduction scenarios were modelled. In these scenarios, anthropogenic ROG or NO_x emissions were individually reduced by 35%. The difference of the ozone concentration for two such model runs yields the ozone limitation ($O_{3\,lim.}$, see definition below). The presented model results are discussed for 13 May 1998 at 15h CET. At this day, the highest photooxidant production was observed during the measuring campaign. In the afternoon, high ozone concentrations of nearly 200 ppb were measured at the semi-rural station Verzago, around 30 km north of Milan. In the area of Milan, such high ozone events develop

ACPD
3, 733–768, 2003

frequently from spring to summer (see also Prévôt et al., 1997).

In Fig. 1, two dotted rectangles are displayed. They denote the urban Milan as well as the "Po Basin". The smaller rectangle represents 3 × 3 grid cells (81 km^2) and the bigger one 21 × 21 grid cells (3969 km^2). The area of the modelling domain is 22 842 km^2. The dashed circle denotes the core of the modelled ozone plume of the cases A–D, F and G at 15:00 CET. In Table 1, the mean of Milan represents the area of the city, including the station Bresso. The "Po Basin" area includes the area of Milan city and the core of the modelled ozone plume at 15:00 CET. Table 1 includes mean concentration of O_3, O_3 of both reduction scenarios, H_2O_2, NO_x and NO_y for Milan and "Po Basin". "Plume" means the according concentrations in the peak of the modelled ozone plume, which is also the highest ozone concentration in the whole modelling domain.

The following sections as well as the figures relate to the numbers in Table 1. The quantification of the ROG and NO_x reductions on the ozone limitation of the different cases (Fig. 2) is expressed as

$$O_{3\,\mathrm{lim.}} = O_3(-35\%\mathrm{ROG}_{\mathrm{anthrop.}}) - O_3(-35\%\,\mathrm{NO_x})$$

$$NO_x \text{ limited} : O_{3\,\mathrm{lim.}} > 0\,\mathrm{ppb};\ \text{ROG limited} : O_{3\,\mathrm{lim.}} < 0\,\mathrm{ppb}.$$

Higher $O_{3\,\mathrm{lim.}}$ refers to higher NO_x sensitivity and lower $O_{3\,\mathrm{lim.}}$ to higher ROG sensitivity in the modelling domain.

Case A: mixing height

The modelled ozone concentrations for the base case (*bc*) in the lowest layer of the LOOP domain for 13 May at 15:00 CET are given in Fig. 2. In the morning during stagnant wind conditions, primary pollutants were accumulated near Milan and formed a photochemical plume in the late morning hours. Afterwards, the ozone plume moved slowly northward, reaching nearly 200 ppb ozone close to Verzago.

Figure 3a shows the influence of the enhanced mixing height on the modelled ozone concentration in the two areas and on peak ozone. The changes lead to a significant

decrease of the ozone concentration, especially in peak ozone. At 15:00 CET, the modelled peak ozone drops from 195 ppb to 169 ppb to 134 ppb when increasing the mixing height from 1000 to 1500 to 2000 m a.g.l. (−31%). In addition, the extension of the region with more than 130 ppb ozone shrinks in A2 to one third of the original 40 km extension. Doubling the mixing height leads to a mean ozone reduction in Milan of 19.5% and in the "Po Basin" of 14%. Enhancing the mixing height twice by 500 m leads to non-linear reduction in the ozone concentration in Milan and ozone plume (Fig. 3a). In the "Po Basin", the ozone reduction seems to linearly depend on the mixing height changes.

Not only the ozone concentration is decreasing with increasing mixing height in variation A1 and A2 due to a greater dilution in the mixing layer, but also the NO_x and NO_y concentrations. In *bc*, the highest amount of total reactive nitrogen (NO_y) is found in the ozone plume. In A2, NO_y concentration in the core of the ozone plume is reduced by 51%. The H_2O_2 concentration, however, increases in the whole domain indicating a shift to relatively more NO_x sensitive conditions (Fig. 4a), as is also reported by Li et al. (1998). The figure displays the number of all NO_x ($O_{3\,\mathrm{lim.}} > 0$ ppb) and ROG ($O_{3\,\mathrm{lim.}} < 0$ ppb) limited grid cells found in the domain for the variations of case A. For *bc*, the number of all NO_x limited grid cells in the domain is 73.6% and the ROG limited amounts to 20.3%. The missing fraction indicates grid cells equal to zero. In addition, the number of NO_x limited grid cells $O_{3\,\mathrm{lim.}} > 5$ ppb and ROG limited grid cells $O_{3\,\mathrm{lim.}} < -5$ ppb are included in the figure to get a measure of increased number of more sensitive grid cells. The changing percentages in Fig. 4a seem to be small, but the relative change of 1% indicates 25 grid cells (228 km^2). In A2, the number of NO_x limited grid cells increases by nearly 3% compared to *bc*. This surface expansion is well notable in the modelled limitations in Fig. 2. In *bc*, the most sensitive ROG area with around $O_{3\,\mathrm{lim.}} = -77$ ppb lies within the highest ozone plume region. In A1 this area is east of the main ozone plume and $O_{3\,\mathrm{lim.}}$ is −52 ppb (not shown). Extending the mixing height to 2000 m, the most sensitive ROG region is slightly more south of the ozone plume with around $O_{3\,\mathrm{lim.}} = -44$ ppb ozone. As a result, the change in mixing

ACPD
3, 733–768, 2003

height is too weak to change the limitation completely from ROG to NO_x limitation in this case.

Sillman et al. (1995) report a 25% change in NO_y being associated with a 15% change in peak ozone, when reducing the mixing height from 2000 m in the base case to 1200 m a.g.l. in the perturbed cases (personal communication). We found stronger NO_y and O_3 decreases with increasing mixing height.

Case B: temperature

At constant specific humidity, the modelled ozone production at the given time is almost linearly dependent on the temperature (solid lines in Fig. 3b). The linear regression coefficients of the temperature dependence of the modelled ozone concentrations of case B at 15:00 CET are given in Table 3. In Milan a slope of 2.8 ppb/° C is found. The strongest gradient is found in the ozone plume with 10.1 ppb/° C. As a result, the ozone production efficiency with increasing temperature is about 3.6 times higher in the ozone plume than in Milan, which reflects mostly the inflow conditions south of Milan. Along with the higher concentrations, the extension of the ozone plume (cross-section at the level 130 ppb) in variation B1 is around 70 km compared to 40 km in *bc*.

Generally, higher temperatures alter the chemical reaction rates. These higher temperatures are related to an enhanced decomposition of peroxyacetylnitrate (PAN) and higher homologues (Sillman et al., 1990; Sillman and Samson, 1995; Vogel et al., 1999; Wunderli and Gehrig, 1991). The equilibrium between NO_2 and PAN (and its homologues) is shifted to higher NO_2 concentrations at higher temperatures. With increasing temperature of case B, the formation of PAN in the modelling domain is reduced and is most pronounced in the ozone plume. In *bc*, the modelled PAN concentration at 15:00 CET is 13.1 ppb, while the concentration in B1 decreases to 6.4 ppb. The NO_2 concentration in the ozone plume of *bc* is about 12 ppb and in B1 9.6 ppb. Simultaneously, the HNO_3 concentration in the ozone plume of the latter case increases to 25.9 ppb compared to 20.8 ppb in *bc*. The change in PAN production is the most important reason for the enhanced ozone production at higher temperatures. If PAN is

formed less, more radicals are available to react with NO to form NO_2 which produces ozone. In the NO_x sensitive production, also the higher NO_x concentrations favour higher ozone production.

The total reactive nitrogen (NO_y) concentration at Milan is nearly insensitive to the temperature rise. The urban air shows relatively fresh primary emissions (NO_x), which are not yet photochemically transformed into secondary pollutants and the reduced formation of PAN leads to an increase of the NO_x concentration. A different picture shows the ozone plume, where the photochemically aged air indicates decreasing NO_x concentration in spite of the lower PAN production. The reduction must be due to higher ozone concentration (+46%), yielding higher OH and thus nitric acid formation. Additionally, the NO_2 deposition is higher. The removal by dry deposition of the increasing HNO_3 appears to determine the decreasing NO_y concentration with increasing temperature. In the "Po Basin", the H_2O_2 and NO_x concentration increases moderately with increasing temperature, while the NO_y concentration slightly decreases due to the enhanced HNO_3 dry deposition removal.

The number of ROG limited grid cells increases by 25% comparing B1 with *bc*. The NO_x limited areas $O_{3\,\mathrm{lim.}} > 5$ ppb decrease from 94 grid cells (*bc*) to only 15 grid cells in variation B1. Hence, the modelling domain tends to get less NO_x limited. The ROG sensitivity is $O_{3\,\mathrm{lim.}} = -92$ ppb in B1 compared to $O_{3\,\mathrm{lim.}} = -77$ ppb in *bc* (Fig. 2). However, the ozone concentration is higher (285 ppb) compared to 195 ppb in *bc*.

Increasing air temperature leads to increased biogenic emissions in reality. Dommen et al. (2002) derived from measurements especially for the Po Basin a low contribution (~6%) of biogenic emissions to the ROG reactivity. The biogenic emission contribution to the ROG reactivity in the modelled ozone plume is also low (~4.7%). For this reason, the changes in biogenic emissions are not expected to strongly alter the effect on the limitation in case B, which otherwise would foster NO_x limitation.

Different calculated slopes in case B and D (same as case B, but with strongly increased humidity amount) are compared with slopes determined from measurements in Milan and Mendrisio. The latter monitoring site is found about 18 km northwest of

ACPD
3, 733–768, 2003

Verzago and is similarly frequently as Verzago affected by polluted air masses stemming from Milan.

Weber et al. (2002) analysed the daily ozone maximum in Mendrisio and correlated them with temperatures. If one defines days with (ozone maximum) – (ozone concentration at noon) >40 ppb as plume days, one finds 10 ppb ozone/° C for temperatures between 20 and 30° C. The value of 40 ppb is arbitrary, but seems to be a reasonable limit for the differentiation (Weber et al., personal communication). Analysing the ozone concentration found in the PIPAPO database for Milan for ozone concentrations >60 ppb and temperatures between 20 and 30° C results in a slope of 5.8 ppb/° C (Table 3). Usually with increasing temperature the background ozone concentration will also change in reality. This fact is not taken into account in the model, where the boundary conditions remain the same for all simulations. Especially the calculated slope in the model for Milan would therefore be higher because the ozone background is a much higher fraction of the ozone concentration in Milan than in the ozone plume. The calculated slopes in case D are very similar to case B, indicating that the strong humidity increase has a minor effect on the dependence of the ozone concentration on temperature.

Case C: specific humidity

The model simulation of case C were performed using the original temperature input file but with variations of the specific humidity (C1–C8). Changing the water content influences the availability of OH radicals and subsequently the ozone production. An excited oxygen atom is formed by photolysis of ozone through reaction (1).

$$O_3 \rightarrow O_2 + O(^1D). \quad (1)$$

Increasing the water content in reaction (2) leads to an increased formation rate of OH radicals.

$$H_2O + O(^1D) \rightarrow 2OH. \quad (2)$$

ACPD
3, 733–768, 2003

OH may react with ROG and carbon monoxide forming peroxy radicals (RO_2 and HO_2), converting NO to NO_2 and leading to a net ozone formation. Hence, ozone concentrations may increase with increasing humidity, if this enhanced production is higher than the ozone destruction by photolysis and reactions of ozone with radicals.

Figure 3c shows for the two areas and the ozone plume about a linear increase of ozone concentration with inclining humidity (C8–C1: 80%). In Milan and the "Po Basin", the incline in ozone is very weak at the given time with 1.2% and 2.7%, respectively. The ozone plume shows the strongest ozone increase with enhanced humidity (13%).

A strong decrease of hydrogen peroxide with decreasing humidity in the whole domain is found. A change of the specific humidity by 80% (from C1 to C8) yields a mean H_2O_2 decrease in the ozone plume of −46%, in Milan of −44.4% and in the "Po Basin" area of −37.5%. The NO_x concentrations in Milan, "Po Basin" and ozone plume increase with decreasing humidity, due to the diminished oxidative capacity of the atmosphere. The NO_x increase is most pronounced in the ozone plume (73%). A slight increase of NO_y with decreasing humidity in all areas is as well found due to less conversion of NO_x to nitric acid. The NO_y increase is most pronounced again in the ozone plume (6%).

Despite the fact that the ozone shows about a linear increase with increasing humidity, the effect on the limitation is non-linear. In Fig. 4c, the number of ROG sensitive grid cells $O_{3\,lim.} < 0$ ppb shows a strong increase with decreasing humidity, which is obviously related to higher NO_x and lower peroxide in the modelling domain. The ROG sensitive grid cells $O_{3\,lim.} < -5$ ppb increase as well strongly, while the NO_x limited grid cells $O_{3\,lim.} > 5$ ppb in the base case drop from around 3% to 0.2% in variation C7. The last number indicates that the domain gets very weak NO_x limited for the benefit of stronger ROG limited areas. Figure 2 shows the limitation of C7.

Vogel et al. (1999) studied in a box model the influence of humidity on the ozone production and transition value of NO_y. In their work, a humidity change from 3.1 to 9.3 g/kg shifted the transition of maximum ozone concentration from 20 ppb to 30 ppb NO_y. Below these levels, ozone increased with decreasing humidity and above, ozone

ACPD
3, 733–768, 2003

increased with increasing humidity. The latter condition is similar to the behaviour of the ozone and NO_y concentrations of case C in the two areas and the ozone plume of the modelling domain. In the NO_x limited areas, ozone increases with decreasing humidity. Note, that the humidity enhancement in this case covers a comparable humidity range as described by (Vogel et al., 1999).

Case D: temperature and specific humidity

The variations in case D are represented by a combination of altered temperatures and water contents of the input files. As is denoted in Sect. 4, the specific humidity supplements in the perturbed input files was calculated based on the varied temperatures ensuring that 95% relative humidity was not exceeded during night. The temperature enhancements in cases B and D are the same, whereas the total amount of humidity in D is strongly increased compared to case C. The observed effects of the latter case on the ozone concentration in the two areas and the ozone plume are included in Fig. 3b (dashed lines), allowing to compare the results directly with case B.

Even with the increased formation rate of OH, only a small additional incline of the ozone formation is found – in the urban area it is hardly noticeable. The combined changes in case D on the NO_y concentrations are comparable to case B, but with a slightly decreased NO_y level in all areas. The effect on the NO_x concentrations in Milan are also comparable to case B, but with a slightly declined level (ΔNO_x: 0.2–0.7 ppb). In the ozone plume and "Po Basin", the enhanced humidity and chemical reaction rates leads to stronger and faster NO_x decrease compared to case B. The H_2O_2 formation strongly increases in case D in the whole modelling domain. Comparing the two areas and the ozone plume, the increase is most pronounced in the ozone plume with 500% from *bc* to variation D1 (Milan and "Po Basin": 100%)! According to this, the NO_x limited areas are expected to grow with enhanced temperature and humidity (Fig. 4d). The number of NO_x limited grid cells in the modelling domain is indeed enhanced by 5.8% comparing *bc* and variation D1. The ratio of all ROG limited grids decrease accordingly, as well as the number of the $O_{3\,\mathrm{lim.}} < -5$ ppb ROG limited grid cells.

In Fig. 2, the modelled limitation of the variation D1 is given. It clearly shows that the NO_x limited areas are increased compared to B1. North of the point source of Turbigo, the ROG sensitive area influenced by this point source is now isolated and not merged any more with the ROG sensitive urban plume area.

Concluding from the model results of the individual temperature (case B) and humidity variations (case C) compared to the combined variations in case D, the net ozone formation in northern Italy is more strongly temperature than humidity dependent. Higher temperature yields rather more ROG sensitive conditions, while increased humidity is leading to more NO_x sensitivity. In our combined case D, the effect of humidity is stronger yielding more NO_x limited conditions in spite of higher temperatures.

Case E: wind speed

The preparation of the input file for the model simulations with regard to enhanced wind speeds is described in Sect. 4. Assuming that the formation of the ozone plume takes place during the stagnant morning hours by accumulation of primary pollutants, enhanced wind speeds before 12:00 CET were chosen to provoke a greater dilution of primary pollutants in the modelling domain. In Fig. 3d, the changes in ozone concentration for the chosen two areas and new ozone plume are given. The most pronounced ozone change is found in the ozone plume. The primary emissions in Milan in the morning hours of E1 are distributed over a greater area and are further transported to the west of Milan city before the ozone plume turns north to the Alps reaching peak ozone of 168 ppb at 15:00 CET. In a comparable simulation to E1, but where all available wind input information in SAIMM were doubled after 12:00 CET, peak ozone in UAM-V reaches 172 ppb at the same given time. In this variation, the ozone plume was similarly formed as in *bc*, but is transported faster and further to the north during the afternoon. Enhancing the wind speeds by a factor of 2 during the whole day reduces peak ozone formation to 151 ppb. In variation E2, no distinct ozone plume is formed, rather two areas with enhanced O_3 concentrations (not shown), whereas peak

ACPD
3, 733–768, 2003

ozone is reached at 17:00 CET. The changes in ozone concentration in Milan and "Po Basin" are lower than 10 ppb comparing *bc* with E2, while the ozone plume indicate a change of around 70 ppb. As a result, the ozone concentration in the whole modelling domain gets more evenly distributed and in addition gets more dominated by the boundary conditions with increased wind speeds.

In Fig. 4e, the number of all NO_x ($O_{3\,lim.} > 0$ ppb) and ROG ($O_{3\,lim.} < 0$ ppb) limited grid cells of case E are given. Enhanced wind speeds change the ROG limited areas from 20.3% to 24% comparing *bc* with E2. The according NO_x limited areas change from 73.6% to 69.9%. Moreover, both NO_x sensitive ($O_{3\,lim.} > 5$ ppb) and ROG sensitive areas ($O_{3\,lim.} < -5$ ppb) strongly decrease.

Analysing the limitations without point sources reveal an interesting feature. The ROG and NO_x limited areas for this base case are 79.1% and 14.7%, respectively (Fig. 4f). Simulating E1 without point sources results now in a total number of NO_x and ROG limited grid cells of 84.8% and 15.2%, respectively, pointing to an increased number of NO_x limited grid cells! Hence, the point sources demonstrate a strong ROG sensitive influence on the modelling domain. Concluding, the treatment of point sources in model simulations can reverse the dependence of the ROG/NO_x limitation on wind speed changes.

In our model simulations, we found that enhanced wind speeds are indicative of greater dilution of polluted plumes as indicated by Biswas and Rao (2001). Sillman et al. (1995) report 10% change in simulated peak O_3 and 15% change in concurrent NO_y concentration associated with enhanced wind speeds. Our model leads to a 15% reduction in peak ozone and 41% NO_y when doubling the morning wind speeds.

Case F and G: Enlarging the spatial resolution of the emission inventory

Enlarging the spatial resolution of the emission inventory reduces the emission variability because highest emission grid cells are averaged with surrounding grid cells. Emissions increase in the latter ones, due to the levelling. The simple applied resampling technique of the original emission inventory is described in Sect. 5. An example

ACPD
3, 733–768, 2003

of the highest NO emission variation in Milan with respect to the changed spatial resolution is also given there (Table 2). The lower emission strength in the city emission grid cells leads to a reduced ozone formation in the ozone plume (Fig. 3e, solid line), which changes highly non-linear by 19.5% from base case to variation F3 ($54 \times 54\,km^2$). The emission levelling results in a broadening of the modelled ozone plume with applied coarser emission inventories. In Milan and "Po Basin", a gradual increase of the ozone concentration with coarser emission inventory due to the averaged emissions is found. The modelled ozone distribution for variation F1 ($9 \times 9\,km^2$) is almost not discernible from *bc*, which is shown in Fig. 2.

The mean ozone concentration of case G – without point sources – is included in Fig. 3e (dashed lines) and compared to case F. The impact of point sources in the Milan and "Po Basin" area and ozone plume is small (<4 ppb). However, local ozone destruction of > −30 ppb and > −10 ppb is found where the point sources of Tavazzan and Turbigo influence the modelling domain.

A change of −36% NO_y and −70% of NO_x is found in Milan enlarging the spatial resolution of the emission inventory from $3 \times 3\,km^2$ to $54 \times 54\,km^2$. The reduction of NO_y in the ozone plume is more pronounced (−47%) than in Milan and "Po Basin" (−13%). The change of NO_x in the ozone plume is −57%, while a −42% change is observed in the "Po Basin". As a result, the greatest changes are found enlarging the spatial resolution of the emission inventory from $27 \times 27\,km^2$ (F2) to $54 \times 54\,km^2$ (F3). The H_2O_2 concentration in Milan, "Po Basin" and ozone plume is mostly insensitive to coarser emissions. However, a strong change in the ozone plume is observed from variation F2 to F3 (+55%).

Reducing the spatial resolution leads to an enhanced number of NO_x limited grid cells in the model (Fig. 4f). Cases F and G are both included in Fig. 4f, showing the differences when excluding the point sources in the model simulations. The number of the NO_x limited grid cells change from *bc* to variation F1 by 2.2% to 75.8% and from *bc* to variation G3 by 4.9% to 84%, where the greatest changes occur again between $27 \times 27\,km^2$ and $54 \times 54\,km^2$. No ROG $O_{3\,lim.} < -5$ ppb grids are found in variation G3

ACPD
3, 733–768, 2003

($54 \times 54\,km^2$).

In Fig. 2, the ozone concentrations and the calculated limitations for the grid resolution of $27 \times 27\,km^2$ (case F) and $54 \times 54\,km^2$ (case G) are given. The use of a coarser emission inventory not only enhances the number of NO_x limited grid cells but also leads to a less detailed resolution of observed features. Maximum $O_{3\,lim.} > 0$ ppb hardly changes when applying a coarser emission inventory: It remains between about 8–10 ppb. However, the maximum $O_{3\,lim.} < 0$ ppb tends to get much smaller (G2 ($O_{3\,lim.} = -36$ ppb)) nearly reaching 0 ppb (G3 ($O_{3\,lim.} = -1.3$ ppb)). In variation F3, the visible ROG limited areas are only due to the ozone plumes of the point sources.

Kumar et al. (1994) applied a multiscale air quality model with three different grid resolutions ($5 \times 5\,km^2$, $10 \times 10\,km^2$ and $20 \times 20\,km^2$) on southern California. Thunis (2001) used the three dimensional Eulerian TAPOM (Transport and Air Pollution Model) in the Po Basin for the same time period in 1998. He applied a comparable emission inventory to the not modified original emission inventory used in Ritter et al. (2002) and reduced the spatial resolution from $4 \times 4\,km^2$ to $10 \times 10\,km^2$ and $50 \times 50\,km^2$. In both works of Kumar et al. (1994) and Thunis (2001), a uniform enlarging of the spatial resolution of the emission inventory yielded higher levels of urban ozone, similar to our findings. The latter author also reports reduced peak ozone due to coarser emission inventories. However, his base case do not compare with other model simulations (Martilli et al., 2002; Bärtsch-Ritter et al., 2003).

Concluding, coarser grid sizes lead not only to different ozone concentrations but also to influences on the limitation, which obviously may lead to incorrect control strategies. Hence, the grid size of a chosen modelling domain should be carefully evaluated.

7. Conclusions

The three-dimensional photochemical model UAM-V is used to investigate the effects of various meteorological conditions and different spatial emission resolutions on the ozone concentration and ROG/NO_x limitation in the Milan region in the northern part of

Italy during the intensive measuring campaigns of PIPAPO. The quantification of ROG and NO_x reductions on the ozone limitation is described in Sect. 4.6.

Seven cases A–G are designed, for which the input files of the base case (*bc*) were varied. The results of the variations in two defined areas (Milan and "Po Basin") and the ozone plume - expressed as tendency of increasing NO_x or ROG limited areas, increasing ozone, H_2O_2, NO_2 and NO_y concentrations – are given as a summary in Table 4. The arrows do not take the power of the tendency into account. Table 5 shows for selected variations the quantification of the NO_x and ROG limited areas. Most of the undertaken variations lay within possible meteorological conditions that could occur from spring to autumn. The main findings of all cases concerning the limitation are:

Case A: An increase of the mixing height leads to a slight increase of NO_x limited areas in the whole modelling domain, but no dramatic change in the limitation in the various areas is observed.

Case B: The ROG limited areas increase with higher temperatures, mostly because of lower PAN formation at higher temperatures.

Case C: Increased humidity leads to strongly increased NO_x limited areas.

Case D: Higher temperature yields rather more ROG limited conditions, while increased humidity leads to NO_x limitation. In this case, the effect of humidity is stronger yielding more NO_x limited areas in spite of higher temperatures.

Case E: With increasing wind speed, emissions get more evenly distributed in the whole modelling area and gets more influenced by the boundary conditions. Increasing ROG limited areas with increasing wind speed are found, while simulations without point sources tend to increase NO_x limited areas. Hence, the treatment of point sources in model simulations can reverse the dependence of the ROG/NO_x limitation on wind speed changes.

Case F and G: The NO_x limited areas increase with coarser emissions. Excluding point sources in the model simulations lead to stronger increased NO_x limited areas than with point sources.

The model results show that changes in meteorological input files have the largest

ACPD
3, 733–768, 2003

effect on peak ozone. The temperature dependence on the ozone formation in the model results and in measurements was compared. In the modelled ozone plume and in Milan, slopes of 10.1 ppb ozone/° C and 2.8 ppb ozone/° C were found, whereas slopes of 10 ppb ozone/° C and 5.8 ppb ozone/° C were found in measurements. Increased background concentrations with increasing temperatures were not taken into account in the model simulations, possibly explaining the difference between model and measurements.

The net ozone formation in northern Italy is more strongly temperature than humidity dependent, while the humidity is very important for the ROG/NO_x formation of the ozone production. The calculated slopes in case D are very similar to case B, also indicating that the strong humidity increase has a minor effect on the dependence of the ozone concentration on temperature.

For each of the meteorological variations (e.g. doubling the mixing height), the modelled ozone plume remains ROG limited on 13 May. A strong change towards NO_x sensitivity in the ROG limited areas was only found if much coarser emission inventories were applied. It is advisable to perform model simulations in the Po Basin with a spatial grid resolution better than $10 \times 10\,km^2$. The influence of point sources on the limitation in the Po Basin and Milan is important. In model simulations, one should be aware about a potential influence of point sources on the limitation, which may reverse the dependence of the ROG/NO_x limitation on wind speed.

False conditions in meteorological input files and reduced spatial grid resolutions will not only effect modelled species concentrations, but also the limitation, which may lead to incorrect control strategies. Hence, attention should be paid on observation close input files in photochemical simulations in addition to careful considerations regarding grid size of future modelling domains.

Based on the results of this work, we recommend for the Milan region to reduce ROG emissions in urban areas to decrease the highest ozone concentrations.

Acknowledgement. We would like to thank the LOOP community for contributing to the necessary information on measurement data, emissions and boundary concentrations. We also like

to acknowledge comments to this work by Th. Peter and B. Vogel.

References

Andreani-Aksoyogly, S. and Keller, J.: Influence of meteorology and other input parameters on levels and loads of pollutants relevant to energy systems: a sensitivity study, In: Air Pollution IV, Monitoring, Simulation and Control, edited by: B. Caussade, H. Power and C. A. Brebbia (28–30 August 1996), 769–778, 1996.

Atkinson, R., Baulch, D. L., Cox, R. A., Hampson, R. F., Kerr, J. A., Rossi, M. J., and Troe, J.: Evaluated kinetic, photochemical and heterogeneous data for atmospheric chemistry. 5. IUPAC, J. Phys. Chem. Ref. Data, 26, 3, 521–1011, 1997.

Bärtsch-Ritter, N., Prévôt, A. S. H., Dommen, J., Andreani-Aksoyoglu, S., and Keller, J.: Model study with UAM-V in the Milan are (I) during PIPAPO: Simulations with changed emissions compared to ground and airborne measurements, Atm. Env., submitted, 2003.

Biswas, J. and Rao, S. T.: Uncertainties in episodic ozone modelling stemming from uncertainties in the meteorological fields, J. Appl. Met., 40, 117–136, 2001.

Bloomfield, P., Royle, J. A., Steinberg, L. J., and Yang, Q.: Accounting for meteorological effects in measuring urban ozone levels and trends, Atm. Env. , 30, 17, 3067–3077, 1996.

Brönnimann, S., Buchmann, B., and Wanner, H.: Trends in near-surface ozone concentrations in Switzerland: the 1990s, Atm. Env. , 36, 17, 2841–2852, 2002.

Brönnimann, S. and Neu, U.: Weekend-weekday differences of near-surface ozone concentrations in Switzerland for different meteorological conditions, Atm. Env., 31, 8, 1127–1135, 1997.

Davis, J. M., Eder, B. K., Nychka, D., and Yang, Q.: Modeling the effects of meteorology on ozone in Houston using cluster analysis and generalized additive models, Atm. Env., 32, 14/15, 2505–2520, 1998.

Dommen, J., Prévôt, A. S. H., Neininger, B., and Bäumle, M.: Characterization of the photooxidant formation in the metropolitan area of Milan from aircraft measurements, J. Geophys. Res., 10.1029/2000JD000283, 2002.

Dommen, J., Prévôt, A. S. H., Bärtsch-Ritter, N., Maffeis, G., Longoni, M. G., Grüebler, F., and Thielmann, A.: High resolution emission inventory of the Lombardy region: Development and comparison with measurements, Atm. Env., submitted, 2003.

Gery, M. W., Whitten, G. Z., Killus, J. P., and Dodge, M. C.: A photochemical kinetics mechanism for urban and regional scale computer modelling, J. Geophys. Res., 94, A2, 1211–1562, 1989.

Jang, J.-C. C., Jeffries, H. E., Byun, D., and Pleim, J. E.: Sensitivity of ozone to model grid resolution - I. Appliction of high-resolution regional acid deposition model, Atm. Env., 29, 21, 3085–3100, 1995.

Keller, J., Ritter, N., Andreani-Aksoyoglu, S., Tinguely, M., and Prévôt, A. S. H.: Unexpected vertical profiles over complex terrain due to the incomplete formulation of transport processes in the SAIMM/UAM-V air quality model, Environmental Modelling & Software, 17, 747–762, 2002.

Khalid, I. A.-W. and Samson, P. J.: Preliminary sensitivity analysis of Urban Airshed Model simulations to temporal and spatial availability of boundary layer wind measurements, Atm. Env., 30, 12, 2027–2042, 1996.

Kumar, N., Odman, M. T., and Russell, A. G.: Multiscale air quality modelling: Application to southern California, J. Geophys. Res., 99, D3, 5385–5397, 1994.

Li, Y., Dennis, R. L., Tonnesen, G. S., Pleim, J. E., and Byun, D.: Effects of uncertainty in meteorological inputs on O_3 concentration, O_3 production efficiency, and O_3 sensitivity to emissions reducions in the Regional Acid Deposition Model, American Meteorological Society, Boston, MA, In: Preprints of the 10th Joint Conference on the Applications of Air Pollution Meteorology with the Air and Waste Management Association, 11–16 January 1998, Phoenix, Arizona, Paper no. 9A.14, 529–533, 1998.

Lin, X., Trainer, M., and Liu, S. C.: On the nonlinearity of the tropospheric ozone production, J. Geophys. Res., 93, D12, 15879–15888, 1988.

Martilli, A., Neftel, A., Favaro, G., Kirchner, F., Sillman, S., and Clappier, A.: Simulation of the ozone formation in the northern Part of the Po Valley, J. Geophys. Res., 10.1029/2001JD000534, 2002.

Neftel, A., Spirig, C., Prévôt, A. S. H., Furger, M., and Stutz, J.: Sensitivity of photooxidant production in the Milan Basin, J. Geophys. Res., 10.1029/2001JD001263, 2002.

Pielke, R. A.: A threee-dimensional numerical model of the sea breeze over south Florida, Monthly Weather Review, 102, 115–139, 1974.

Porter, P. S., Rao, S. T., Zurbenko, I. G., Dunker, A. M., and Wolff, G. T.: Ozone air quality over North America: part II – An analysis of trend detection and attribution techniques, J. Air & Waste Management Association, 51, 283–306, 2001.

Prévôt, A. S. H., Staehelin, J., Kok, G. L., Schillawski, R. D., Neininger, B., Staffelbach, T., Neftel, A., Wernli, H., and Dommen, J.: The Milan photooxidant plume, J. Geophys. Res., 102, 23375–23388, 1997.
Russel, A. and Dennis, R.: NARSTO critical review of photochemical models and modelling, Atmospheric Environment, 34, 2283–2324, 2000.
SAI: User's Guide to the Systems Applications International Mesoscale Model, System Applications International, Inc., San Rafael, California (SYSAPP-95/070), 1995.
SAI: User's Guide to the variable-grid urban airshed model (UAM-V), System Applications International, Inc., San Rafael, California (SYSAPP-99-95/27r2), 1999.
Sillman, S.: The use of NO_y, H_2O_2, and HNO_3 as indicators for ozone-NO_x-hydrocarbon sensitivity in urban locations, J. Geophys. Res., 100, D7, 14175-14188, 1995.
Sillman, S.: The relation between ozone, NO_x and hydrocarbons in urban and polluted rural environments, Atm. Env., 33, 1821–1845, 1999.
Sillman, S., Al-Wali, K. I., Marsik, F. J., Nowacki, P., Samson, P. J., Rodgers, M. O., Garland,L. J., Martinez, J. E., Stoneking, C., Imhoff, R., Lee, J. H., Newman, L., Weinstein-Lloyd, J., and Aneja, V. P.: Photochemistry of ozone formation in Atlanta, GA-Models and measurements, Atm. Env., 29, 21, 3055–3066, 1995.
Sillman, S., Logan, J. A., and Wofsy, S. C.: The sensitivity of ozone to nitrogen oxides and hydrocarbons in regional ozone episodes, J. Geophys. Res., 95, D2, 1837–1851, 1990.
Sillman, S. and Samson, P. J.: Impact of temperature on oxidant photochemistry in urban, polluted rural and remote environments, J. Geophys. Res., 100, D6, 11497–11508, 1995.
Sistla, G., Zhou, N., Hao, W., Ku, J.-Y., and Rao, S. T.: Effects of uncertainties in meteorological inputs on urban airshed model predictions and ozone contro strategies, Atm. Env., 30, 12, 2011–2025, 1996.
Thunis, P.: The influence of scale in modelled ground level ozone, Norwegian Meteorological Institute, July 2001 (Research Report no. 57), 1–42, 2001.
Vogel, B., Riemer, N., Vogel, H., and Fiedler, F.: Findings on NO_y as an indicator for ozone sensitivity based on different numerical simulations, J. Geophys. Res., 104 D3, 3605–3620, 1999.
Weber, R. and Prévôt, A. S. H.: Climatology of ozone transport from the free troposphere into the boundary layer south of the Alps during North Foehn, J. Geophys. Res., 107, D3, 10.1029/2001JD000987, 2002.
Wolff, G. T., Dunker, A. M., Rao, S. T., Porter, P. S., and Zurbenko, I. G.: Ozone air quality over

ACPD
3, 733–768, 2003

north America: Part I – A review of reported trends, Journal of Air & Waste Management Association, 51, 273–282, 2001.
Wunderli, S. and Gehrig, R.: Influence of temperature on formation and stability of surface PAN and ozone. A two year field study in Switzerland, Atm. Env., 25A, 8, 1599–1608, 1991.

Table 1. Compilation of mean O_3, H_2O_2, NO_x and NO_y concentration in the two defined areas of Milan and "Po Basin" (Fig. 1) and the according concentrations in the ozone plume for all variations of the cases A–G valid for 13 May 1998 at 15:00 CET. For the cases B, C, and D, only the base case and the extreme variation results are shown

Variation		O_3			O_3 (-35% ROG)			O_3 (-35% NO_x)			H_2O_2			NO_x			NO_y		
		Milan	Plume	Po Basin	Milan	Plume	Po Basin	Milan	Plume	Po Basin	Milan	Plume	Po Basin	Milan	Plume	Po Basin	Milan	Plume	Po Basin
Mixing height (m a.g.l.)																			
A2	2000	93.0	134.4	101.8	91.5	112.2	97.5	96.5	129.5	102.5	2.0	1.2	1.7	21.5	6.1	8.3	33.3	23.7	19.7
A1	1500	101.1	168.7	109.8	99.4	129.1	104.9	104.1	159.5	109.7	1.9	1.3	1.6	21.9	7.4	8.6	35.1	33.5	21.8
bc	1000	115.5	195.0	118.4	113.0	133.7	112.4	118.2	196.1	118.5	1.6	0.9	1.5	23.1	12.5	9.7	38.3	46.3	23.9
ΔT (°C)																			
B1	10	141.9	285.3	144.7	137.6	190.8	134.5	144.5	263.3	143.7	2.0	2.5	1.8	24.4	9.9	10.2	38.5	42.2	23.6
bc	0	115.5	195.0	118.4	113.0	133.7	112.4	118.2	196.1	118.5	1.6	0.9	1.5	23.1	12.5	9.7	38.3	46.3	23.9
B7	-4	103.9	162.0	107.1	101.9	112.6	102.4	106.8	175.8	108.0	1.4	0.7	1.3	22.5	16.2	9.7	38.5	48.7	24.3
Δq (%)																			
C1	20%	115.4	200.7	118.8	113.1	138.1	112.9	117.8	194.7	118.3	1.8	1.1	1.6	22.9	10.9	9.5	38.3	45.8	23.8
bc	0	115.5	195.0	118.4	113.0	133.7	112.4	118.2	196.1	118.5	1.6	0.9	1.5	23.1	12.5	9.7	38.3	46.3	23.9
C8	-60%	114.0	177.2	115.6	111.0	119.3	109.1	118.7	200.0	118.4	1.0	0.6	1.0	23.8	18.9	10.9	38.5	48.7	24.3
ΔT (°C), Δq (%)																			
D1	10, +110%	142.5	290.2	147.3	138.6	231.2	138.8	143.5	256.1	143.1	3.2	5.4	3	23.7	8.3	9.1	38.2	40.7	23.1
bc	0, 0%	115.5	195.0	118.4	113.0	133.7	112.4	118.2	196.1	118.5	1.6	0.9	1.5	23.1	12.5	9.7	38.3	46.3	23.9
Wind speed (enhancement)																			
bc	* 1	115.5	195.0	118.4	113.0	133.7	112.4	118.2	196.1	118.5	1.6	0.9	1.5	23.1	12.5	9.7	38.3	46.3	23.9
E1	* 2	108.1	164.8	116.2	106.7	135.6	112.5	112.8	152.2	116.8	1.6	1.2	1.4	22.9	5	9.3	37.4	27.5	22.9
E2	* 5	105.6	127.2	111.3	104.6	116.3	109.4	110.8	133.1	112.6	1.7	0.8	1.5	21.4	10.7	9.2	35.9	27.3	22.4
Spatial resolution of the emission inventory (km^2) (emissions including point sources)																			
bc	3 x 3	115.5	195.0	118.4	113.0	133.7	112.4	118.2	196.1	118.5	1.6	0.9	1.5	23.1	12.5	9.7	38.3	46.3	23.9
F1	9 x 9	118.5	192.3	119.9	116.1	133.1	113.7	120.1	192.5	119.6	1.6	0.9	1.4	21.8	11.8	9.5	37.3	44.5	23.9
F2	27 x 27	125.3	182.1	124.1	121.8	137.7	116.6	126.2	175.3	122.5	1.4	1.1	1.4	15.4	7.9	8.6	31.4	35.2	23.5
F3	54 x 54	142.1	156.8	128.7	136.9	143.5	123.2	136.1	143.7	123.5	1.4	1.7	1.5	6.9	5.4	6.0	24.4	24.6	20.9
Spatial resolution of the emission inventory (km^2) (emissions without point sources)																			
bc	3 x 3	115.4	197.8	117.6	112.9	135.7	112.1	118.2	191.3	116.5	1.6	1.0	1.6	23.1	10.9	8.9	38.3	44.1	22.6
G1	9 x 9	118.5	194.1	119.3	116.1	135.1	113.5	120.1	187.7	117.6	1.6	1.0	1.6	21.8	10.2	8.7	37.3	42.2	22.6
G2	27 x 27	125.2	182.9	123.8	121.7	140.3	116.9	126.2	169.9	120.5	1.4	1.2	1.5	15.4	6.6	7.7	31.4	33.0	22.2
G3	54 x 54	142.0	152.6	128.0	136.9	143.1	123.7	136.1	136.9	121.1	1.4	2.0	1.6	6.9	5.1	5.2	24.4	22.7	19.7

ACPD
3, 733–768, 2003

Table 2. Variation of the maximum NO emission (g/h) in Milan for selected hours and different spatial resolutions of the used modified emission inventory

Milan

hour (CET) / spatial resolution (km^2)	2 - 3	8 - 9	14 - 15	20 - 21
3 x 3	1077	6651	5507	2784
9 x 9	316	4432	3652	1770
27 x 27	154	2136	1819	863
54 x 54	73	825	708	341

Table 3. Calculated slopes (ppb ozone /° C temperature) from measurements and from model results for cases B (temperature variations) and D (temperature and humidity variations) at different sites. Please see text for further explanation

	Model		Measurements	
Regression	Plume	Milan	Mendrisio	Milan
Slopes case B	10.1	2.8	10	5.8
r^2	0.99	0.99	0.6	0.44
Slopes case D	10.8	2.7		
r^2	0.99	0.99		

ACPD

3, 733–768, 2003

Table 4. The results of cases A–G are expressed as tendency of increasing NO_x or ROG limited areas in the modelling domain and of increasing ozone, H_2O_2, NO_2 and NO_y concentrations in the two different denoted areas Milan and "Po Basin" and the ozone plume. Note, that the power of the tendency is not taken into account

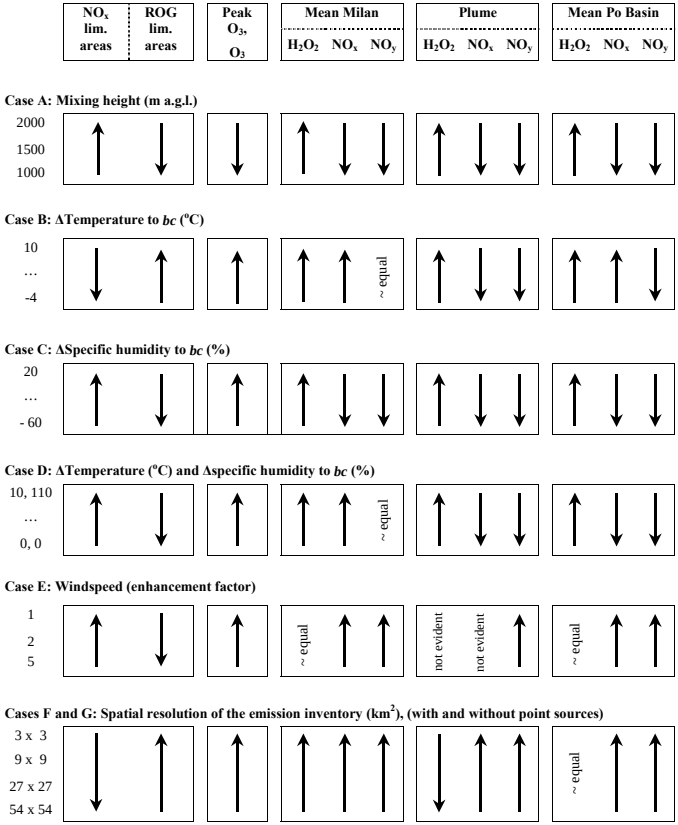

ACPD
3, 733–768, 2003

Effects of various meteorological conditions and spatial emission resolutions

N. Bärtsch-Ritter et al.

Table 5. Fraction of NO_x and ROG limited grid cells in whole modelling domain for selected variations valid for 15:00 CET

	Description	Fraction of NO_x limited area (%)	Fraction of ROG limited area (%)
base case (*bc*)	Emission including point sources	73.6	20.3
base case*	Emission *without* point sources	79.1	14.7
A2	*mixing height at 2000 m a.g.l.*	76.4	17.4
B1	ΔT= 10 °C of *bc*	68.4	25.4
B7	ΔT= -4 °C of *bc*	73.1	20.7
C1	Δspec. humidity = +20 % of *bc*	76.2	17.7
C8	Δspec. humidity = -60 % of *bc*	59.3	34.5
D1	ΔT= 10 °C and Δspec. humidity = +110 % of *bc*	79.4	14.5
D5	ΔT= 2 °C and Δspec. humidity = +20 % of *bc*	75.8	18.1
E2	*wind speed enhancement *5*	69.9	24
F1	9 x 9 km^2 spatial resolution of emission inventory	75.1	20.3
F3	54 x 54 km^2 spatial resolution of emission inventory	75.8	18.0
G1*	9 x 9 km^2 spatial resolution of emission inventory	80.9	12.6
G3*	54 x 54 km^2 spatial resolution of emission inventory	84.0	9.8

ACPD
3, 733–768, 2003

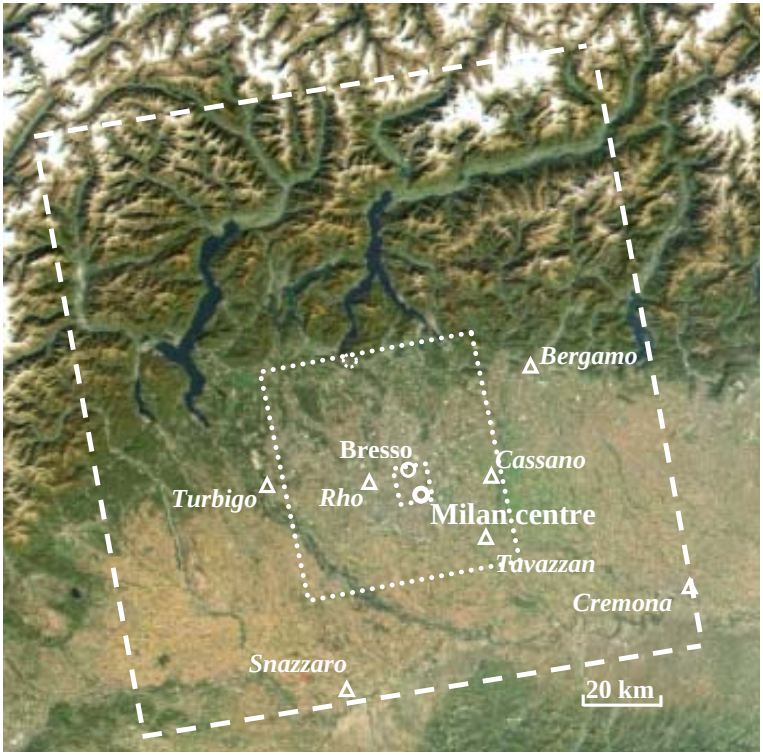

Fig. 1. Area of investigation in the northern part of Italy. Circles indicate Milan centre and the urban station Bresso. Triangles denote point sources. The smaller square represents the area of Milan centre including station Bresso. The dashed circle denotes the core of the modelled ozone plume of the cases A–D, F and G at 15:00 CET. The bigger square is denoted as "Po Basin" including the area of Milan and the core of the ozone plume. Different concentrations in the core of the ozone plume and means within the squares are calculated and compiled in Table 1.

ACPD
3, 733–768, 2003

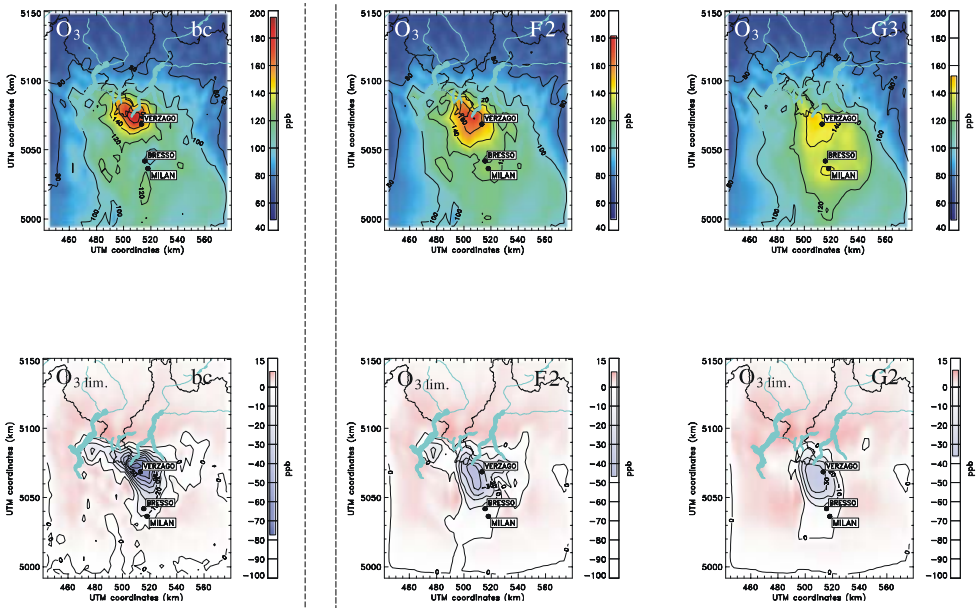

Fig. 2. Modelled ozone concentration and limitation for base case (*bc*) and selected variations given at 15 h CET. Variations G2 and G3 are modelled without point sources.

ACPD
3, 733–768, 2003

Effects of various meteorological conditions and spatial emission resolutions

N. Bärtsch-Ritter et al.

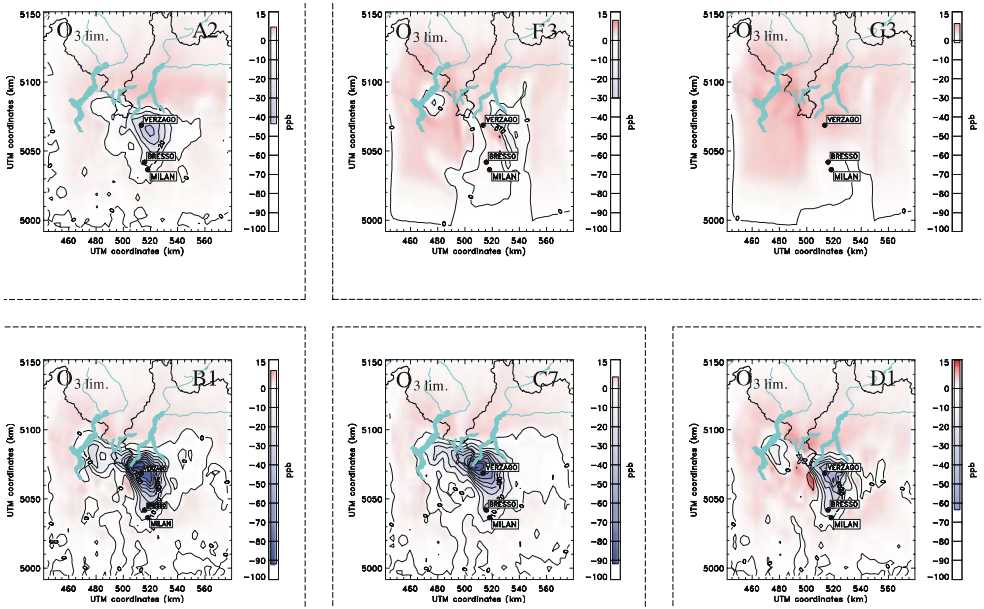

Fig. 2. Continued.

ACPD
3, 733–768, 2003

Effects of various meteorological conditions and spatial emission resolutions

N. Bärtsch-Ritter et al.

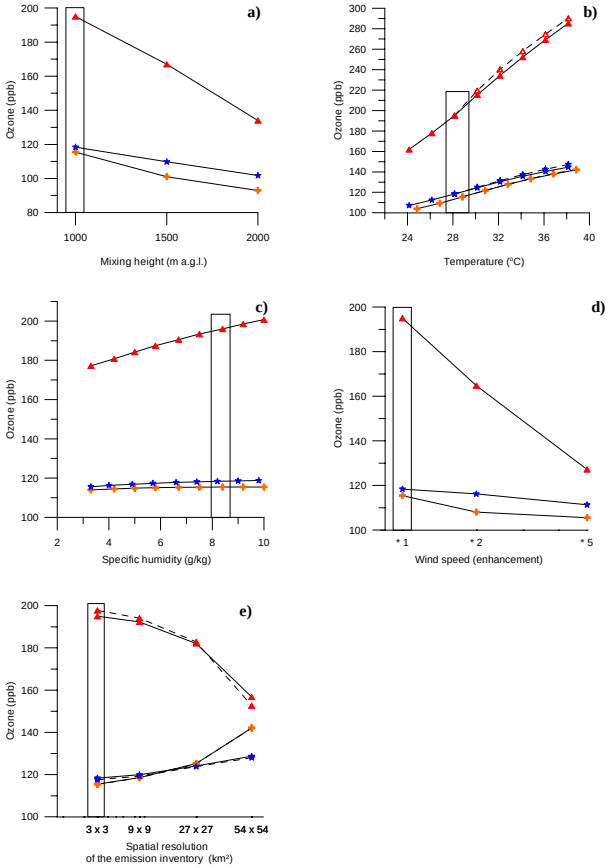

Fig. 3. Peak ozone (triangles) and mean ozone concentrations in the two denoted areas of Milan (crosses) and "Po Basin" (stars) for the cases A–G. **(b)** includes cases B (temperature variations, solid lines) and D (temperature and humidity variations, dashed lines). Cases F (variations of the spatial resolution of the emission inventory including point sources, solid lines) and G (ditto, but without point sources) are compiled in **(e)**.

ACPD
3, 733–768, 2003

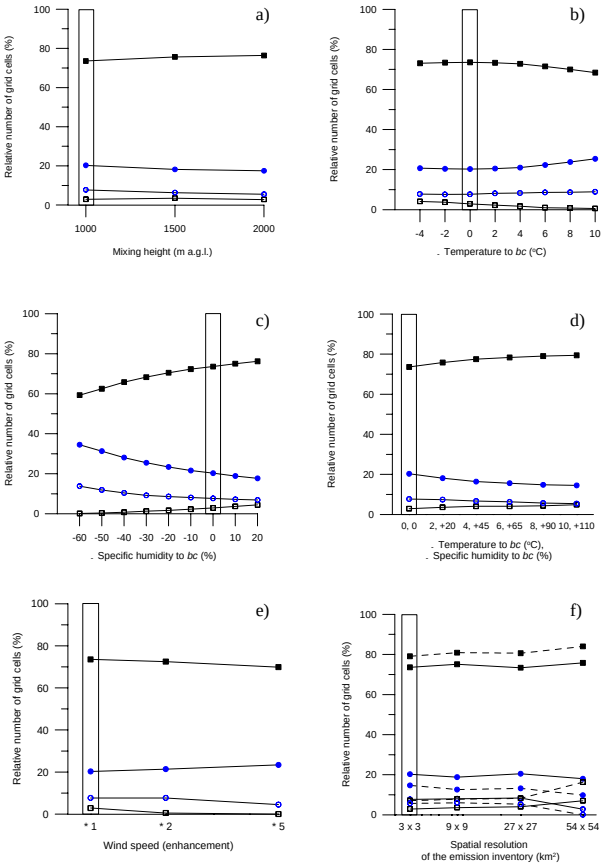

Fig. 4. Fraction of NO_x (filled squares) and ROG (filled circles) limited grid cells in whole modelling domain for cases A–G. Unfilled symbols indicate NO_x sensitive grid cells $O_{3\,lim.} > 5$ ppb and ROG sensitive grid cells $O_{3\,lim.} < -5$ ppb. Cases F (variations of the spatial resolution of the emission inventory including point sources, solid lines) and G (variations of the spatial resolution of the emission inventory without point sources, dashed lines) are compiled in **(f)**.

ACPD
3, 733–768, 2003